NUMERICAL SIMULATION OF MODEL HELICOPTER ROTOR IN HOVER

PIOTR DOERFFER AND OSKAR SZULC

Institute of Fluid-Flow Machinery PAS,
Fiszera 14, 80-952 Gdansk, Poland
{doerffer, osmark}@imp.gda.pl

Abstract: The article presents details of a URANS simulation of the flow field near a hovering model of the Caradonna and Tung (1981) helicopter rotor [1]. The CFD code SPARC [2] proves to be capable of capturing the aerodynamics of a two-bladed rotor in high-speed transonic hover conditions. A comparison of the simulation results with the experimental data is acceptable, hence the described methodology might be used with confidence in future numerical studies of application of noise-reducing devices on helicopter blades.

Keywords: transonic, hover, helicopter rotor

1. Introduction

A normal shock wave, terminating a local supersonic area on the rotor blade of a helicopter not only limits aerodynamic performance but also becomes a significant source of a high-speed impulsive noise. A new passive method of noise reduction by shock wave smearing has already been proposed and tested on a NACA0012 2D profile [3]. This method is based on the local application of a cavity covered by a perforated plate beneath the shock. The resulting flow recirculation through the cavity leads to the substitution of the strong normal shock wave by a more gradual compression, reducing the pressure gradients above the airfoil surface – the main source of noise.

The next step on the path leading to a simulation of a helicopter rotor equipped with a passive control device is to assess the ability of the CFD code to capture a flow field of a "clean" baseline rotor in hover (without perforation). This necessary phase of validation against the available experimental data is the main objective of this article.

It is evident that a full simulation of a helicopter rotor in hover conditions raises many difficulties. A rotating blade creates a high downwash of air below the rotor even far from the rotor plane (Figure 1). A spiral tip and root vortices and the trailing edge vortex sheet interact with the preceding blade by modifying the local effective inflow angle – a key parameter in a simulation of the real blade loading. It
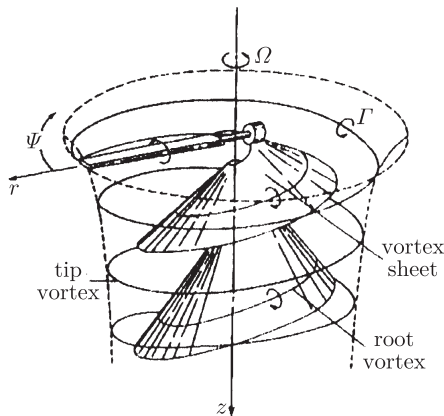
Figure 1. Helicopter rotor wake
of a single blade [4]
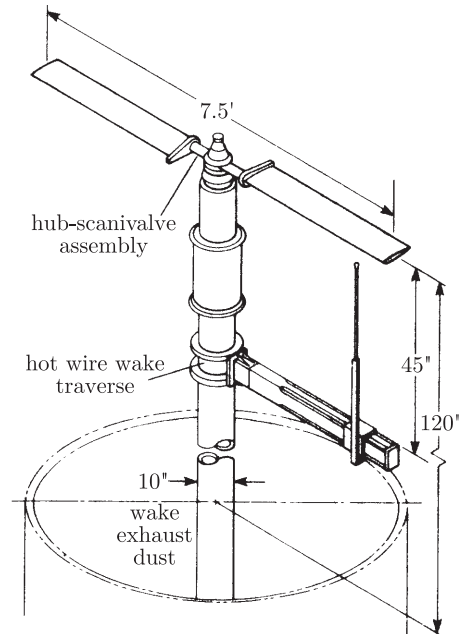
Figure 2. Experimental set-up
of Caradonna-Tung two-bladed
model rotor in hover [1]

is not only a local flow in the vicinity of the blades but also the wake of the rotor itself that has to be sufficiently resolved. A wrong prediction of the rotor wake and tip vortex trajectory leads to an erroneous vertical inflow velocity which results in a large discrepancy with the experimental data.

2. Caradonna-Tung (1981) model helicoper rotor in hover

The CFD code validation is performed against the experimental data obtained by Caradonna and Tung in 1981 [1]. This test-case is extensively used within the helicopter community for validation of CFD codes applied to rotorcraft problems. RANS solutions to this problem that capture the rotor wake without any need for external wake models are available in the literature [4–10].

The model rotor consists of 2 rectangular, untwisted and untapered NACA0012 rigid blades mounted on a tall column containing a drive shaft located in a large chamber with special ducting designed to eliminate room recirculation (Figure 2). The rotor aspect ratio $\mathrm{AR} = 6$, chord length $c = 0.1905\,\mathrm{m}$ $(0.625\,\mathrm{ft})$ and diameter $2R = 2.286\,\mathrm{m}$ $(7.5\,\mathrm{ft})$. A large set of test conditions has been applied with the tip Mach number ranging from $\mathrm{Ma}_T = 0.226$ to $\mathrm{Ma}_T = 0.890$ and the collective pitch setting of $\Theta = 0°\ldots12°$ at ambient conditions. Pressure distributions have been measured at 5 cross-sections of the blade and tip vortex trajectory has been extracted using a hot-wire technique.

The modelled geometry of the Caradonna-Tung rotor is shown in Figure 3 (aspect ratio $\mathrm{AR} = 6$, chord length $c = 1\,\mathrm{m}$ and diameter $2R = 12\,\mathrm{m}$). No detailed
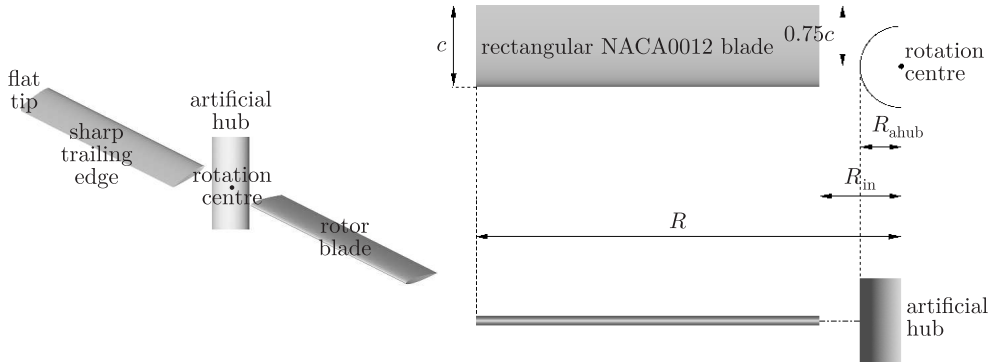
Figure 3. Geometry of Caradonna-Tung rotor (collective pitch $\Theta = 8°$)

Figure 4. Caradonna-Tung rotor blade dimensions (collective pitch $\Theta = 0°$, AR = 6, $c = 1$, $R_{\mathrm{ahub}} = 0.5c$, $R_{\mathrm{in}} = c$, $R = 6c$)

information about the hub geometry or the tip shape is available from the experiment. The computational model utilizes flat tip surfaces and sharp trailing edges for all blades. The artificial hub cylindrical surface of a radius of $R_{\mathrm{ahub}} = 0.5c$ replaces the shaft real shape (Figure 4). It is assumed that the inner radius of the rotor $R_{\mathrm{in}} = c$.

3. Numerical method of solution – SPARC code

The present investigation has been carried out with a cell-centred block-structured CFD code SPARC [2] developed at the University of Karlsruhe in the Fortran 90 programming language supplied with MPI parallel libraries. This code solves numerically compressible, mass-weighted, Reynolds-averaged Navier-Stokes (RANS) equations with several turbulence models. The one-equation low-Reynolds number turbulence model of Spalart-Allmaras proved to be efficient in prediction of the flow field of a hovering rotor. This set of equations is closed by a perfect gas assumption and Sutherland's law binding dynamic viscosity to the temperature field.

The algorithm uses a semi-discrete approach, utilizing a finite-volume, density-based formulation for spatial discretisation (central scheme, 2$^{\mathrm{nd}}$ order of accuracy) and explicit Runge-Kutta type method for integration in time (CFL number of 5). In order to increase the convergence rate, the local time stepping and the implicit residual averaging techniques are included in the explicit approach. The full multigrid strategy with V-cycles additionally improves the convergence rate. For a time accurate simulation an efficient implicit dual-time-stepping scheme (1$^{\mathrm{st}}$ order of accuracy) has permitted utilization of all acceleration techniques developed for explicit algorithms. The artificial dissipation scheme SLIP is incorporated into the code to damp numerical oscillations .

4. Computational domain – grid topology and boundary conditions

The computational domain of the Caradonna-Tung rotor is divided into 80 structured blocks (Figures 5 and 6) with a C-topology in streamwise and H-topology

in normal and spanwise directions. The C-H-H topology proves to be able to capture the rotor wake system in contrast to the O-O topology. Unfortunately, the large outer blocks collapse near the axis of rotation into a very small volume that may lead to the instability of the numerical algorithm. The hovering rotor flow field is quasi steady with respect to the blade and periodic in nature – only one blade needs to be accounted for, decreasing the time requirements for the simulation.
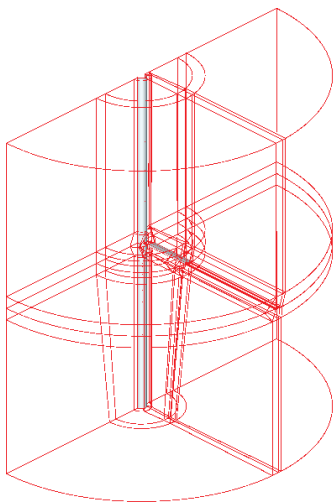
Figure 5. Multi-block topology for a single blade of Caradonna-Tung rotor, 80 blocks
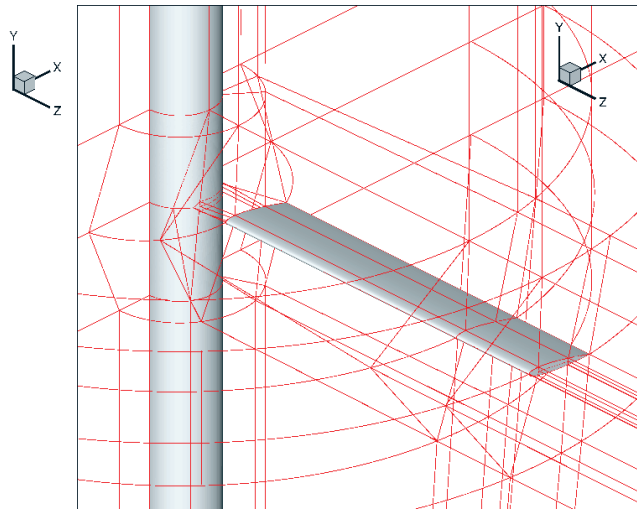
Figure 6. Multi-block topology for a single blade of Caradonna-Tung rotor, blade close-up

A computational body-fitted structured grid is generated semi-automatically using parameterised python scripts inside the IGG (Numeca) software. It consists of 5.7 million of volumes for a single blade (Figures 7 and 8). The distance of the first grid point from a solid wall is of the order of $y^+ = 1$ in the whole domain. The grid clustering is enforced not only at the boundary layer development locations, but also in the rotor wake and on the path of the tip and root vortices. In Figure 9 a cut through the grid at $r/R = 0.8$ projected on $z = $ const plane is presented showing mesh orthogonality and smoothness.

The computational domain is surrounded by boundary conditions of 4 types: viscous and inviscid walls, rotational periodicity and pressure inlet/outlet (Figure 10). The surface of the blade is modelled using a no-slip condition with a zero heat-flux (adiabatic wall) – grey colour. Since the flow is periodic, a rotational periodicity boundary condition is used (rotation: axis 0 1 0, point 0.25 0 0 and angle of 180°) – red colour. To save computational resources a surface of the artificial hub is modelled as an inviscid wall – green colour. The farfield surface (located $3R$ away from the axis of rotation in every direction) is approximated by a pressure inlet/outlet boundary condition – blue colour. It is based on the assumption of constant inlet total pressure and temperature far from the blades. At the rotor wake exhaust locations this condition is automatically switched into an outlet with imposed static pressure.
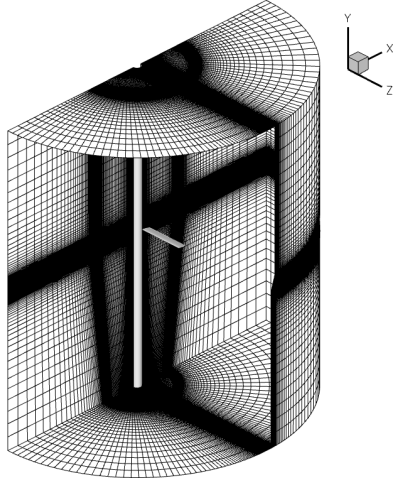
Figure 7. Structured C-H-H cylindrical grid for Caradonna-Tung rotor, 5.7 million of volumes
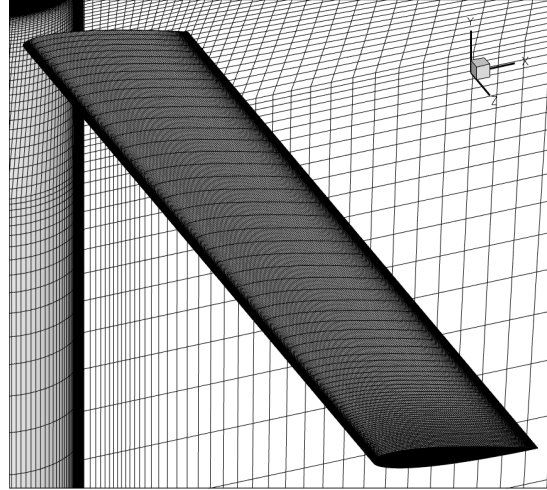
Figure 8. Structured C-H-H cylindrical surface grid for Caradonna-Tung rotor, blade close-up
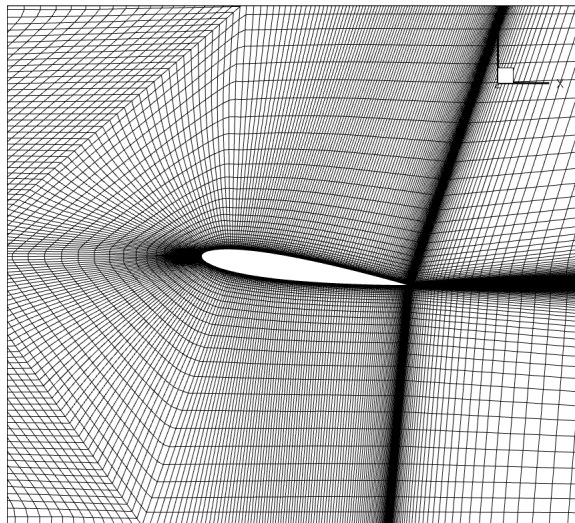
Figure 9. Structured C-H-H cylindrical grid for Caradonna-Tung rotor, cut at $r/R = 0.8$ projected on $z = \mathrm{const}$ plane

The rotor is placed in a quiescent environment with ambient pressure and temperature (P_{atm} and T_{atm}). When the blades are rotating with a positive collective pitch Θ a non-zero velocity is induced at the boundaries. At locations where air is moving into the computational domain (inlet), the ambient conditions P_{atm} and T_{atm} become stagnation parameters for the entering flow. At outlet (below the rotor) where the air is leaving the computational domain, static pressure is equal to ambient pressure P_{atm}. It is possible because the blades add energy to the fluid changing its stagnation parameters.
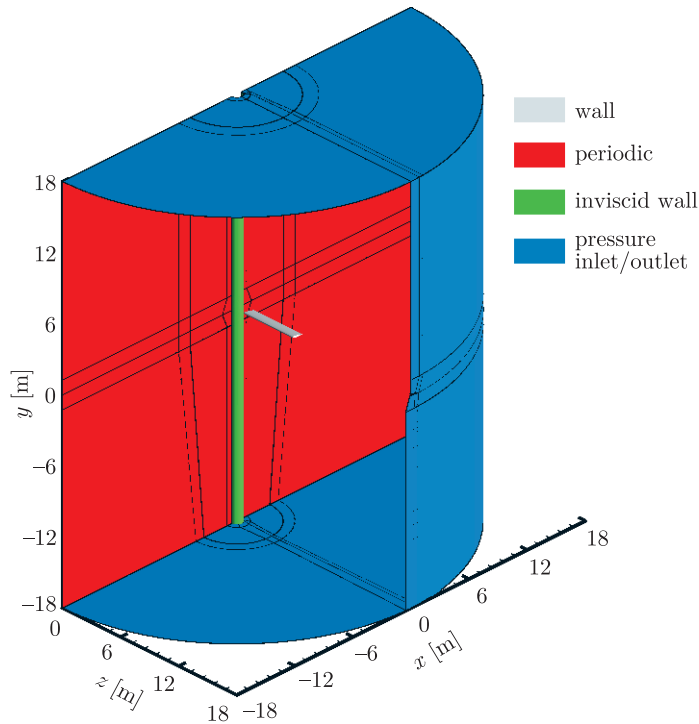
Figure 10. Boundary conditions for Caradonna-Tung rotor

For the purpose of SPARC code validation, a transonic test-case with experimental tip Mach number equal to $Ma_T = 0.877$, tip Reynolds number of $Re_T = 3.931 \cdot 10^6$, rotation speed of 2500 rpm (frequency of $f = 41.67$ Hz) and a collective pitch of $\Theta = 8°$ has been chosen. In order to keep a desired tip Mach and Reynolds number using a blade with a larger chord length ($c = 1$ m), the physical parameters need to be modified. The values used as an input to the boundary conditions in the simulation are summarized in Table 1.

Table 1. Caradonna-Tung rotor simulation – a summary of geometrical and flow conditions

parameter	experiment	CFD
chord length c [m]	0.1905	1
aspect ratio AR	6	6
tip Mach number Ma_T	0.877	0.877
tip Reynolds number Re_T	$3.93 \cdot 10^6$	$3.93 \cdot 10^6$
tip velocity U_T [m/s]	299.24	299.24
collective pitch Θ [°]	8	8
frequency f [Hz]	41.667	7.9375
ambient pressure P_{atm} [Pa]	103 027	19 627
ambient temperature T_{atm} [K]	289.75	289.75
ambient density ϱ_{atm} [kg/m^3]	1.2389	0.23602

The inlet total pressure/temperature boundary condition requires additional parameters apart from the numbers in Table 1. Two flow angles have to be assumed – in XY plane ($-90°$) and XZ plane ($0°$). The Spalart-Allmaras 1-equation turbulence model also requires specification of the inlet laminar to turbulent viscosity ratio (set to $\mu_T/\mu = 1$). The temporal accuracy is assured by a choice of a sufficiently small time step $\Delta t = 2 \cdot 10^{-3}$ s giving approximately 62 time steps per one period of rotation ($5.8°$ per 1 iteration).

5. Results of Caradonna-Tung rotor in hover simulation

A fully turbulent unsteady simulation of the flow field of the Caradonna-Tung rotor in high speed hover requires approximately 3000 implicit dual time stepping steps ($\Delta t = 2 \cdot 10^{-3}$ s) on the finest grid to reach a quasi-steady solution. Thrust coefficient C_T and drag coefficient C_D exhibit only small scale oscillations with a mean value independent on time. The experimental value of $C_T = 0.00473$ is underpredicted by 1 % and equal to $C_T = 0.00469$. The loading distribution along the span of the blade exhibits only a small deviation from experimental data (located mainly on the outer 20 % of the blade – in a transonic flow region), Figure 11. To compare the sectional thrust it has been necessary to integrate the experimental and numerical pressure distributions using the same numerical method.
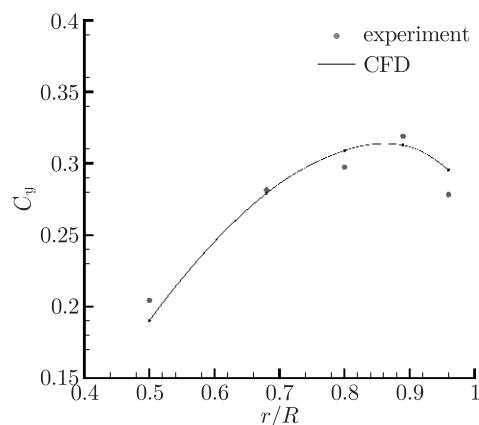
Figure 11. Loading of the rotor blade (sectional thrust)

One of the most important aspects of the simulation of a rotor in hover conditions is proper capturing of the rotor wake and the tip vortex path. The important thing in the current simulation is that the wake of the rotor is not set externally, but it is a part of the global solution. In Figure 12 the surface of constant vorticity reveals a tip vortex which is generated at the tip of the blades and follows a contracting helical shape. This contracted wake descends slowly and remains in close proximity to the blades. There is a strong induced velocity field associated with the tip vortex that significantly alters the effective angle of attack seen by the rotor. This interference plays a dominant role in the vortex wake formation and directly affects the rotor performance.

Figure 12. Isosurface of vorticity, aerodynamic wake of the Caradonna-Tung rotor
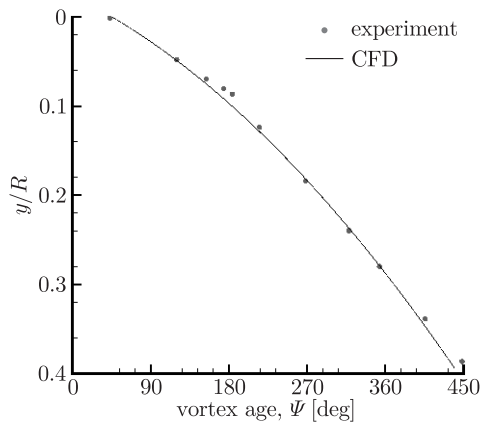
Figure 13. Tip vortex descent
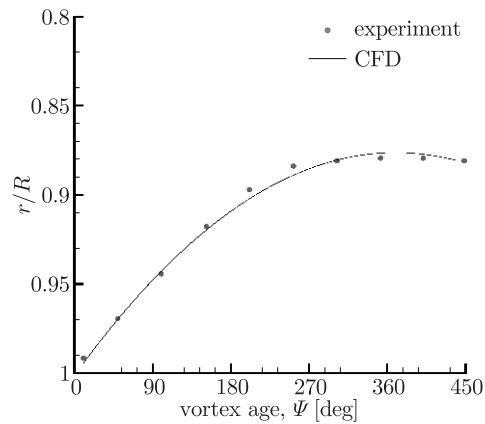
Figure 14. Tip vortex contraction

The RANS method using structured grids is known to be very dissipative and to produce a tip vortex that is diffused very soon (in contrast to the automatic mesh adaptation or the chimera technique). Approximately 450° of a tip vortex age is resolved in the current simulation which is sufficient to capture the most important interaction of the shed vortex with the following blade. Nevertheless, the tip vortex descent and contraction rates (both based on the location of maximum vorticity) are accurately predicted by the current method (Figures 13 and 14).

A more detailed insight into the flow behaviour may be obtained by comparing the pressure coefficient C_P distribution with the experimental data at 5 cross-sections along the span of the blade ($r/R = 0.5$, 0.68, 0.80, 0.89 and 0.96), Figures 15–19. At $r/R = 0.5$ and 0.68 the flow is fully subsonic, while a shock system is building up on the outer 20% of the blade ($r/R = 0.80$, 0.89 and 0.96). It is worth noticing that the shock location is predicted correctly in accordance with the measurements for all transonic radial locations. The vertical rotor wake (vertical inflow) affects mainly the inner part of the blade, where only small velocities are induced by rotation. At the outer part of the blade the rotation velocity dominates. The overall agreement with experimental data is
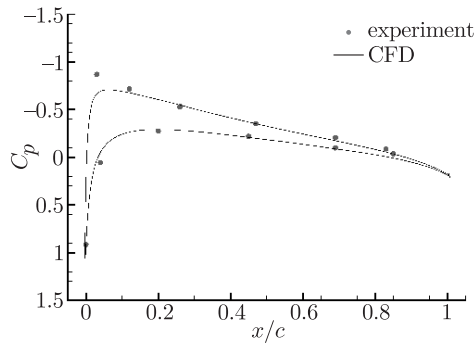
Figure 15. Pressure coefficient C_P distribution at radial location $r/R = 0.5$
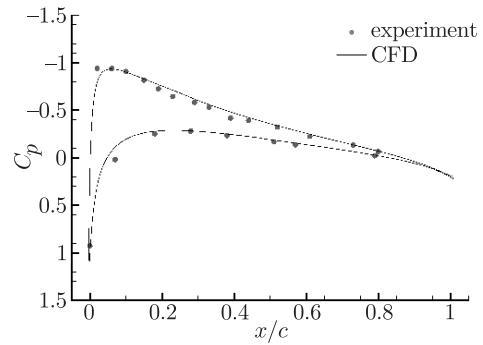
Figure 16. Pressure coefficient C_P distribution at radial location $r/R = 0.68$
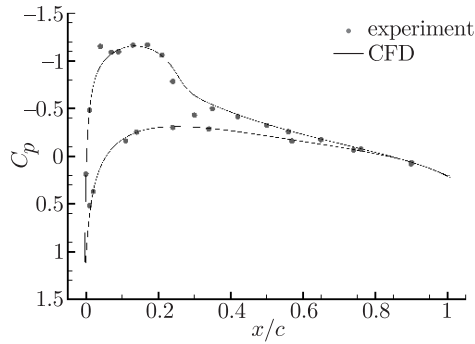
Figure 17. Pressure coefficient C_P distribution at radial location $r/R = 0.80$
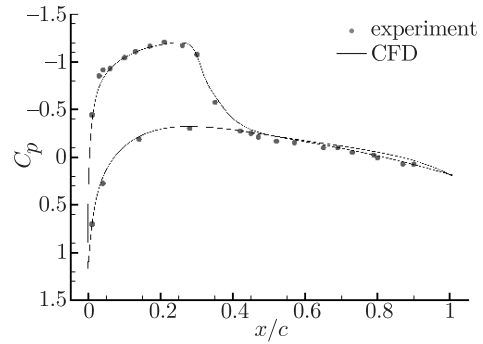
Figure 18. Pressure coefficient C_P distribution at radial location $r/R = 0.89$
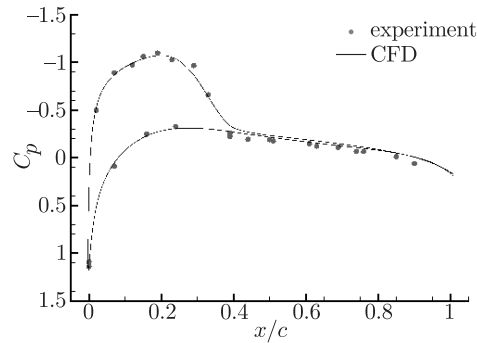
Figure 19. Pressure coefficient C_P distribution at radial location $r/R = 0.96$

satisfactory, excluding the leading edge acceleration at $r/R = 0.5$ and the lack of small, shock-induced separation bubble noticeable in the pressure distribution at $r/R = 0.80$.

6. Conclusions

We have proven that a numerical method implemented in the SPARC code is capable of predicting a flow field of a hovering Caradonna-Tung rotor in transonic

conditions. In the next step, the SPARC code will be applied to the passive control of the shock wave by wall perforation and the high-speed impulsive noise reduction.

References

[1] Caradonna F X and Tung C 1981 *Experimental and Analytical Studies of a Model Helicopter Rotor in Hover*, NASA Technical Memorandum 81232
[2] Magagnato F 1998 *TASK Quart.* **2** (2) 215
[3] Doerffer P and Szulc O 2006 *Archives of Mechanics* **58** (6) 543
[4] Conlisk A T 2001 *Progress in Aerospace Sciences* **37** 419
[5] Steijl R, Barakos G N and Badcock J 2006 *Eur. Conf. on Computational Fluid Dynamics ECCOMAS CFD*, Delft, The Netherlands
www.numerical.rl.ac.uk/people/marioli/Archives/ECCOMAS-CFD-2006/documents/8.pdf
[6] Srinivasan G R, Baeder J D, Obayashi S and McCroskey W J 1990 *Flowfield of a Lifting Hovering Rotor – A Navier-Stokes Simulation*, NASA Technical Memorandum 102862
[7] Majety K S 2003 *Solutions to the Navier-Stokes Equations in a Non-Inertial Reference Frame*, MSc Thesis, Mississippi State University, USA
[8] Hill J L 2005 *The Development of a Boundary Layer Transition Model for Helicopter Rotor CFD*, PhD Thesis, Cranfield University, USA
[9] Hariharan N and Sankar L N 2000 *A Review of Computational Techniques for Rotor Wake Modelling* **AIAA-00–0114**
[10] Usta E 2002 *Application of a Symmetric Total Variation Diminishing Scheme to Aerodynamics of Rotors*, PhD Thesis, Georgia Institute of Technology, USA